Numerical modeling of free-surface wave effects on flexural vibration of floating structures

†Shahrokh Sepehrirahnama, Eng Teo Ong, Heow Pueh Lee, and Kian-Meng Lim

Department of Mechanical Engineering, National University of Singapore, Singapore.

†Corresponding and presenting author: mpeshse@nus.edu.sg

Abstract

To investigate flexural vibration of structures in a fluid, a numerical algorithm was developed to relate the added mass and damping effects of the fluid to each mode of vibration. These are separate from the traditional added mass associated with rigid body motion, such as the translational motion along Cartesian axes. In this formulation, small-amplitude free surface waves were accounted for by using a non-singular implementation of the free-surface Green's function for a potential flow solver based on Boundary Element Method. The formulation was applied to the free and forced vibration of structures, namely a hemispherical shell and a simplified ship model, to obtain their dynamic response at various excitation frequencies. The results show the influence of added damping at lower frequencies as well as the simplicity of relating the fluid added mass to mode shapes of the structures.

Keywords: **Free Surface Wave, Non-singular Boundary Element Method, Fluid-Structure Interaction**

Introduction

For a structure interacting with surrounding fluid, any sudden change in the motion, for example onset of motion or change in the acceleration, results in additional resistance form the fluid in the form of a pressure load. This fluid loading can be represented by an equivalent system of mass and damper, which are called added mass and added damping, respectively [1]-[9]. Added-mass depends on the geometry of the fluid-structure interface, density of the fluid and the type of motion [1]-[3]. Added damping occurs due to the viscosity and condition of the free-surface of the fluid if it exists [4]-[9].

Added-mass and damping have been studied for different geometries of structures, either being fully or partially submerged in a fluid domain, under translational rigid-body motion [4]-[10][14][19][20]. A few studies were reported about relation between the flexural vibration of structures and added mass [21]-[24]. In most of the theoretical studies of applications such as offshore mobile structures (ships or submarines), the fluid or sea water is typically modeled as an incompressible fluid with negligible viscosity; thus, added-damping only arises from the free-surface condition [1][3][5][9][10][14].

For such a case of potential flow, the typical numerical method for calculating the fluid pressure is Boundary Element Method with proper Green's function [3][12][13][15]-[20][24]. The total pressure at the free-surface of the fluid is set to zero. If the pressure head due to the gravity is included in the total pressure, the free-surface elevation, and hence the velocity, is related to the unsteady pressure which rises from changes in the motion. For small amplitude oscillatory flow, this relationship is modeled by the Airy wave equation [25]. To use the

Boundary Element Method, modification of the Green's function is required to satisfy the free-surface wave condition. Several studies reported the surface-wave Green's function as an analytical expression which includes semi-infinite integral of the modified Bessel functions [12][13][15]-[18]. Although several analytical derivations for a limited number of simple geometries existed, numerical implementation of this Green's function is challenging due to the singularity of the Bessel function as well as the infinite bound of the integral. The surface-wave Green's function results in complex-valued pressure and velocity [11][16][17].

In this paper, the aim is to investigate the flexural vibration of shell structures interacting with fluid modelled as potential flow. A non-singular formulation is proposed for implementing the surface-wave Green's function. Then, by using the modal superposition, the fluid loading is calculated for each selected mode shape which are derived for the dry-state of structure. The added-mass and damping are represented the real and imaginary parts of the fluid loading, respectively. By including these fluid effects in the vibration equation, the flexural response of the wet-state of the structure can be calculated. The results show that the proposed numerical formulation provides an efficient way of vibration design of ship structures in sea water.

Theory and formulation

Vibration and modal superposition

Vibration of structures is governed by the following equation,

$$\mathbf{M}\ddot{\boldsymbol{x}} + \mathbf{C}\dot{\boldsymbol{x}} + \mathbf{D}\boldsymbol{x} = \boldsymbol{g}(\boldsymbol{x}) + \mathbf{h}, \tag{1}$$

where $\boldsymbol{x}$ is structure displacement vector, $\mathbf{M}$, $\mathbf{C}$ and $\mathbf{D}$ are the structural mass, damping and stiffness matrices, respectively; time differentiation is denoted by the dot ($\dot{}$) operator. The fluid loading on fluid-structure interface, denoted by $\boldsymbol{g}$, is a function of the displacement of the fluid-structure interface. Other external forces are denoted by $\mathbf{h}$. For time harmonic response, $e^{-i\omega t}$, Eq. (1) is written as follow,

$$(-\omega^2\mathbf{M} - i\omega\mathbf{C} + \mathbf{D})\boldsymbol{X} = \boldsymbol{G}(\boldsymbol{x}) + \mathbf{H}. \tag{2}$$

where ω is the circular frequency; $\boldsymbol{X}$, $\boldsymbol{G}$ and $\mathbf{H}$ are the corresponding complex amplitudes. To determine fluid loading $\boldsymbol{G}$ as a function of displacement, the modal superposition technique is applied. First, structure displacement is written as

$$\boldsymbol{X} = \sum_{j=0}^{N} \boldsymbol{\psi}_j\, Q_j = [\boldsymbol{\psi}]\{\boldsymbol{Q}\}, \tag{3}$$

where $\boldsymbol{\psi}_j$ is the jth mode shape of the dry structure, which is called jth dry mode-shape hereinafter, and $\boldsymbol{\psi}_j$ is associated with the jth dry frequency $f_j^{(dry)}$.The participation factor of the jth dry mode in the response is denoted by Q_j. In the literature, $[\boldsymbol{\psi}]$ and $\{\boldsymbol{Q}\}$ are also known as modal matrix and natural coordinates, respectively. Since the dry mode-shapes are linearly independent and orthogonal, a partial fluid loading $\boldsymbol{F_i}$ is calculated for each of them by using the Boundary Element Method, as described in the next subsection. Again by invoking the concept of modal superposition, the total fluid loading is calculated as follows,

$$\boldsymbol{G}(\boldsymbol{x}) = \sum_{j=0}^{N} F_j\, Q_j = [\boldsymbol{F}]\{\boldsymbol{Q}\}. \tag{4}$$

The fluid loading matrix $[\boldsymbol{F}]$ can be replaced by the equivalent system of mass and stiffness as follows,

$$[\boldsymbol{\psi}]^T[\boldsymbol{F}] = \omega^2\mathbf{M}_{\boldsymbol{a}} + i\omega\mathbf{C}_{\boldsymbol{a}} \tag{5}$$

where $\mathbf{M}_a$ and $\mathbf{C}_a$ are the modal added mass and damping, respectively, and $[\boldsymbol{\psi}]^T$ is the transpose of the modal matrix. The sizes of the added mass and damping matrices are the same as the number of selected dry mode-shapes for modal analysis. The advantage of calculating modal added mass and damping is that the magnitude of the fluid loading and its non-uniform distribution over the interface, for the case of flexural vibration, is reported by a single value which appears on the main diagonal of the matrices. The off-diagonal terms indicate the interaction between different dry mode-shapes in terms of the fluid loading.
By pre- and post-multiplying Eq. (2) with $[\boldsymbol{\psi}]$ and using Eq. (3), (4) and (5), one can write

$$\left(-\omega^2\left(\widehat{\mathbf{M}}+\mathbf{M}_a\right)-i\omega\left(\widehat{\mathbf{C}}+\mathbf{C}_a\right)+\widehat{\mathbf{D}}\right)\{\boldsymbol{Q}\}=\widehat{\mathbf{H}} \tag{6}$$

where $\widehat{\mathbf{M}}$, $\widehat{\mathbf{C}}$, $\widehat{\mathbf{D}}$ and $\widehat{\mathbf{H}}$ are the modal structural mass, damping, stiffness and loading, respectively and $\widehat{\mathbf{M}}=[\boldsymbol{\psi}]^T\mathbf{M}[\boldsymbol{\psi}]$. For free vibration analysis, damping terms and external load are ignored and Eq. (6) becomes

$$\left(-\omega^2\left(\widehat{\mathbf{M}}+\mathbf{M}_a\right)+\widehat{\mathbf{D}}\right)\{\boldsymbol{Q}\}=\mathbf{0}. \tag{7}$$

Eq. (7) is an eigenvalue problem from which the frequencies and mode shapes of the immersed structure, which are called wet frequencies and mode-shapes, can be computed. It is noted that the wet mode-shapes are actually calculated by means of the modal superposition and the $\{\boldsymbol{Q}\}$ obtained from Eq. (7).

Flow simulation with free-surface wave

For a linear inviscid and incompressible flow, Navier-Stokes equation is reduced to a potential flow equation, as follows,

$$\Delta\varphi=0 \tag{8}$$

$$p=-\rho_f\dot{\varphi}+\rho_f g z \tag{9}$$

$$\nabla\varphi=\mathbf{v}=\dot{\boldsymbol{x}} \tag{10}$$

where φ is the velocity potential, p is the total pressure, ρ_f is the density of the fluid, g is the gravity acceleration and z is the position along the vertical. Eq. (9) is also known as the linearized Bernoulli's equation and indicates the contribution of the unsteady motion (first term) and the gravity potential (second term) in the total fluid pressure. On the free surface of the fluid (where $p=0$) for an oscillatory flow, one can rewrite Eq. (9) by using Eq. (10), as follows,

$$-i\omega\varphi+\frac{g}{-i\omega}\frac{\partial\varphi}{\partial n}=0|_{@free-surface}, \tag{11}$$

or

$$\frac{\partial\varphi}{\partial n}=\frac{\omega^2}{g}\varphi|_{@free-surface}, \tag{12}$$

where n is the unit normal to the free surface which is in the z-direction in this derivation. Eq. (12) is known as the Airy wave equation that governs small amplitude wave on the free surface of a fluid due to gravity effects on an oscillatory flow. It shows that the velocity potential and its normal derivative are related on the free surface. The wavelength of the surface wave can be obtained as follows,

$$\lambda_f=\frac{2\pi}{\alpha}=\frac{2\pi}{\omega^2}, \tag{13}$$

where α is the wavenumber. Eq. (8) can be represented as a Boundary Integral Equation, as follow,

$$c_p\varphi(\mathbf{x}_p) + \int_S \frac{\partial G(|\mathbf{x}_p-\mathbf{x}_q|)}{\partial n(x_q)}\varphi(\mathbf{x}_q)dS(\mathbf{x}_q) = \int_S G(|\mathbf{x}_p-\mathbf{x}_q|)\frac{\partial\varphi}{\partial n}(\mathbf{x}_q)\, dS(\mathbf{x}_q) \tag{14}$$

where $G(|\mathbf{x}_p-\mathbf{x}_q|)$ is the Green's function, $\mathbf{x}_p$ and $\mathbf{x}_q$ are the positon vectors of point p and q , respectively, c_p is the solid-angle constant, which is 0.5 if point p is on the boundary Γ and 1 if located in the fluid domain. The area of the surface element at point q is denoted by $dS(\mathbf{x}_q)$. Eq. (13) can be solved by using boundary elements on the fluid-structure interface as long as conditions on other boundaries are satisfied by an appropriate Green's function. A modified Green's function was derived to impose the wave condition without discretizing the infinite free-surface [15]-[17]. The analytical expression for this Green's function, which is called the surface-wave Green's function and denoted by G_w, is

$$G_w = \frac{1}{4\pi r} + \frac{1}{4\pi\bar{r}} + \frac{i\alpha}{2}e^{\alpha(z_p+z_q)}\mathrm{H}_0^{(1)}(\alpha R) + I_\infty, \tag{15}$$

where $R = \sqrt{(x_p-x_q)^2+(y_p-y_q)^2}$, $r = \sqrt{R^2+(z_p-z_q)^2}$, $\bar{r} = \sqrt{R^2+(z_p+z_q)^2}$,

$$I_\infty = -\frac{1}{\pi^2}\int_0^\infty \frac{\alpha\mathrm{K}_0(\eta R)}{\alpha^2+\eta^2}\left(\alpha\cos\eta(z_p+z_q) - \eta\sin\eta(z_p+z_q)\right)d\eta. \tag{16}$$

Here, $\mathrm{H}_0^{(1)}$ and K_0 are the zeroth order Hankel function of the first kind and modified Bessel function of the second kind, respectively [17]. Since K_0 is a fast decaying function, the semi-infinite integral in Eq. (16) is computed by using Gauss quadrature method with 61 Gauss points which gives a relative error of less than 0.01%. Also, by using this numerical technique, the singularity at $\eta = 0$ is also avoided. Since both $\mathrm{H}_0^{(1)}$ and K_0 are singular at zero, the choices of $\mathbf{x}_p$ and $\mathbf{x}_q$ that gives $R = 0$ should be treated separately. For this purpose, a non-singular series expansion is proposed based on Newman's derivation to calculate G_w for the case of $R = 0$ [11]. It is noted that the special case of $R = 0$ occurs when the two points are located along a line parallel to the z axis.

From Newman's series derivation for small distances between the two points p and q [11], an alternative formulation was derived to take care of the $R = 0$ singularity of the Bessel functions, as follows,

$$G_w = \frac{1}{4\pi r} + \frac{1}{4\pi\bar{r}} + \frac{i\alpha}{2}e^{\alpha(z_p+z_q)}\mathrm{J}_0(\alpha R) + \mathcal{T}_\infty \qquad \text{for } R < 10^{-3}, \tag{17}$$

$$\mathcal{T}_\infty = -\frac{\alpha}{2\pi}\mathrm{J}_0(\alpha R)e^{(z_p+z_q)}\mathrm{Ei}\left(-(z_p+z_q)\right) + \mathcal{S}_\infty \tag{18}$$

$$\mathcal{S}_\infty = \sum_{n=1}^{\infty}\frac{(-1)^n}{\Gamma(n)^2}\left(\frac{R}{2(z_p+z_q)}\right)^{2n}\sum_{m=0}^{2n-1}\Gamma(2n-m-1)(-1)^m(z_p+z_q)^m, \tag{19}$$

where J_0 is the order zero regular Bessel function, $\Gamma(n)$ is the Factorial function, Ei is the standard Exponential Integral function, written as follows,

$$\mathrm{Ei}(z) = -PV\left(\int_{-z}^{\infty}\frac{e^{-t}}{t}dt\right) \tag{20}$$

with the principal value being denoted by PV. Eq. (17) to (20) provides a non-singular Green's function for $R < 10^{-3}$ and are easy to implement since the Bessel, Factorial and Exponential Integral functions have standard implementation based on reference [26], and are accessible from any standard math library such as GSL for C/C++ programs. It is noted that there is an infinite sum in Eq. (19); however, using more than 5 terms for $R < 10^{-3}$ changes the final value of the sum by less than 0.1%. Hence, the infinite sum is truncated to only five terms for our computer implementation of the non-singular surface-wave Green's function.

Since this Green's function is a complex-valued function, the calculated pressure amplitudes on the fluid-structure interface are also complex values. The real and imaginary parts of the fluid pressure correspond to the added mass and damping, respectively. By multiplying the pressure with surface area, the fluid loading is obtained at the centroid of each element. The force is distributed to the nodes equally due to the linear shape function. Partial fluid loading for the dry mode shapes are assembled in the same order as the mode shapes to obtain the fluid loading matrix $[\boldsymbol{F}]$.

Proposed numerical formulation

To summarize, the steps in the proposed numerical formulation are listed here, as follows.

- Step 1: Extract N dry mode-shapes by using Finite Element analysis of the structure
- Step 2: For each dry mode-shape, calculate the fluid pressure loading by using Boundary Element Method (Eq. (9), (14), (15) and (17))
- Step 3: Extract the equivalent added mass and damping by using Eq. (5)
- Step 4: Solve the free (or forced) vibration by using Eq. (7) (or (6))
- Step 5: Calculate the structure response by using modal superposition, Eq. (3)

The size of the matrices for in Equations (7) and (6) is the same as the number of selected mode shapes which is much smaller than the size of the discretized model. By using the modified Green's functions to include the free-surface wave, the size of the fluid problem which is solved by Boundary Element Method is also kept to a minimal size. In term of computation time, the fluid solver is the most expensive part of this formulation and it is performed for all selected dry mode-shapes.

Simulation Results

Two case studies, a hemispherical shell and a simplified ship model with internal partitions, were considered; numerical results of structural vibration of these two cases based the proposed numerical algorithm are presented. The normalized frequency, which is reported in this section, is defined as

$$f_j^* = f_j a \sqrt{E/\rho} \tag{2}$$

where f_j is the natural frequency of the jth mode, a is a characteristic length of the given geometry, and E and ρ are the mass density and Young modulus of the solid material, respectively. Variables with the unit of length are also normalized by the characteristic length a.

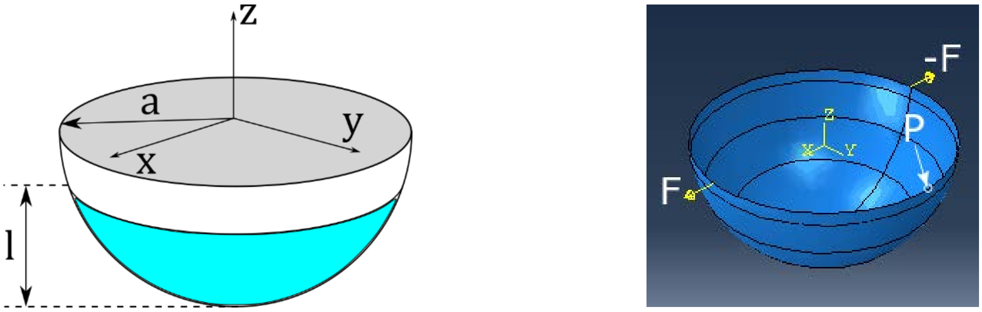

(a) (b)

Figure 1: (a) illustration of a hemispherical shell of radius a, immersed partially by l and

(b) the location of external forces acting on the rim for forced vibration study

Fig. 1 shows the hemispherical shell (case 1) which is immersed by l/a = 0.9, where the immersion depth is denoted by l. The external forces applied to the structure for forced vibration study are shown in Fig. 1b as F. The forces are acting on two opposite points on the rim in the x direction.

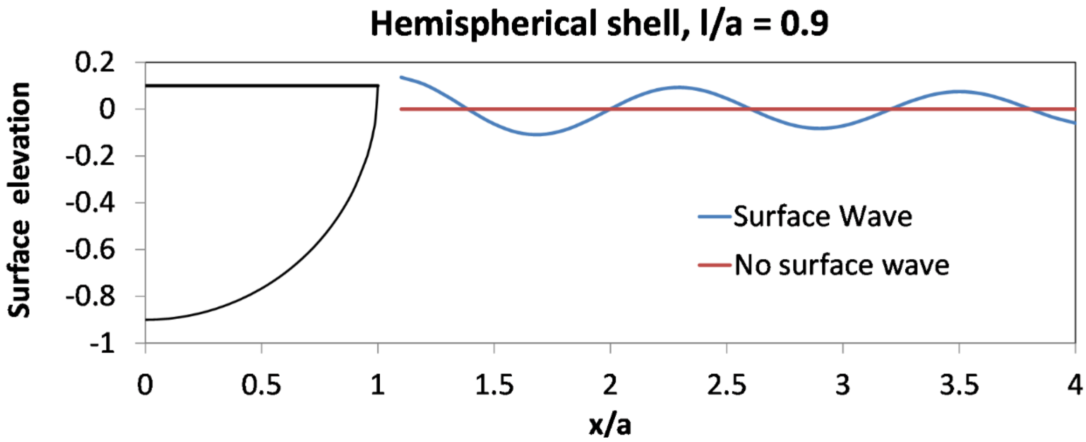

Figure 2: Normalized amplitude of surface elevation along a line segment on the free surface of the fluid domain for two cases, with and without free surface wave. Half of the shell is illustrated at the left side to demonstrate the relative location of the line segment.

For each dry mode-shape of the hemispherical shell, the fluid flow was solved for two scenarios: with and without accounting for the free-surface wave. To verify the implementation of the special Green's function G_w, the normalized amplitude of the surface elevation was plotted for a line segment on the free surface, as shown in Fig. 2, for the first dry mode shape with two nodal lines associated with $f_1^* = 2.20 \times 10^{-4}$. The free-surface wave length was obtained from Eq. (13) to be $1.2a$. The same wavelength can be observed for the surface undulations shown in Fig. 2 This implies that the surface condition is satisfied automatically by using the special Green's function. When the surface wave is neglected, the surface elevation becomes zero, which is presented in Fig. 2 by a red solid line.

After calculating the fluid pressure acting on the hemispherical shell, the added mass and damping were calculated and subsequently incorporated into the vibration equation to obtain the wet frequencies and their associated participation factors from Eq. (7). The wet mode-shapes were then calculated from Eq. (3), by multiplying the participation factors with the modal matrix of the dry structure. Fig. 3 shows the first four dry and wet mode shapes of the shell in ascending sequence of their frequencies. It is noted that the axisymmetric shape of the shell gives the repeated frequencies, for which the corresponding mode shapes have the same number of nodal lines. The same feature was observed for the wet state of the shell, as shown in Fig. 3b and 3d for the first repeated frequencies, and Fig. 3f and 3h for the next pair. Dry mode-shapes were normalized by the unitary normalization technique. The displacement profiles of the wet mode-shapes were derived from the dry mode-shapes and the participation factors. It is noted that the wet mode-shapes are similar to the dry ones, implying that the chosen dry mode-shapes give an appropriate set of basis function to construct the arbitrary response of the shell to any excitation.

As explained in the formulation section, the additional fluid resistance is presented by the modal added mass and damping. For free vibration analysis, only the added mass is accounted for to obtain the wet natural frequencies. The modal added mass matrix is reported in Table 1.

For each mode, the values are normalized by the modal structural mass of that mode. The reported values are rounded up to two decimal places hereinafter.

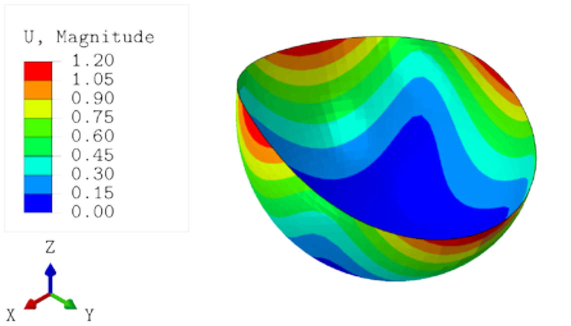

(a) 1st dry mode shape with 2 nodal lines

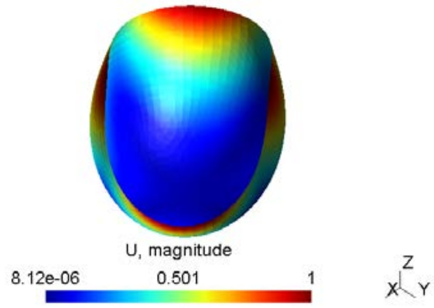

(b) 1st wet mode shape with 2 nodal lines

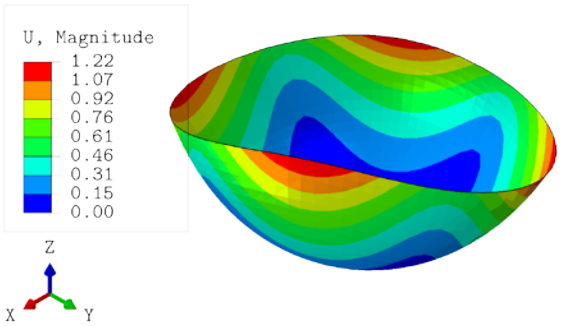

(c) 2nd dry mode shape with 2 nodal lines

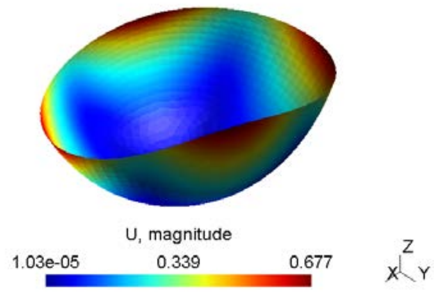

(d) 2nd wet mode shape with 2 nodal lines

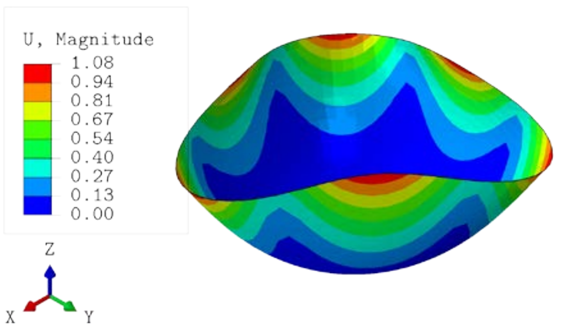

(e) 3rd dry mode shape with 3 nodal lines

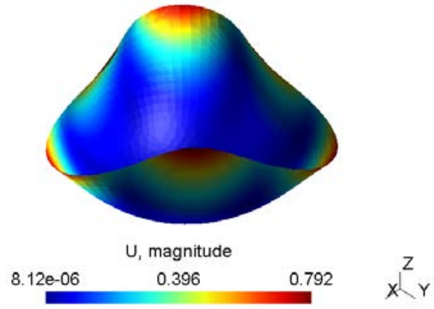

(f) 3rd dry mode shape with 3 nodal lines

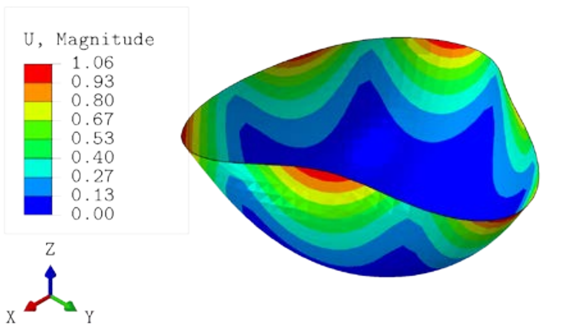

(g) 4th dry mode shape with 3 nodal lines

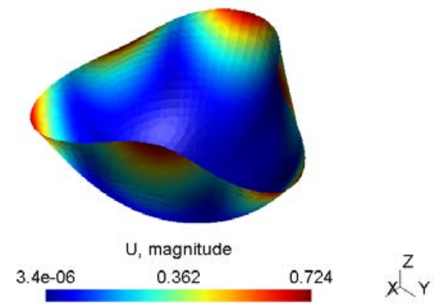

(h) 4th wet mode shape with 3 nodal lines

Figure 3: Panels (a), (c), (e) and (g) are the first four dry mode shapes of a hemispherical shell and panels (b), (d), (f) and (h) are their wet counterparts, respectively, for the immersion depth of $\hat{l} = 0.9$

It is noted that all the diagonal elements are larger than one, indicating that the modal fluid added-mass is larger than structural modal mass. The added mass matrix is not symmetric, due to the formulation of Boundary Element Method used for estimating the fluid loading. Despite the structural added-mass matrix being symmetric, the total mass matrix is non-symmetric which results in non-orthogonal eigenvectors. It was also observed that the off-diagonal elements are smaller than the diagonal ones by at least two orders of magnitude. By solving Eq. (7), wet frequencies and participation factors were computed by using an in-house Eigenvalue solver. The participation factors for the four mode shapes are reported in Table 2 to demonstrate the contribution of each dry mode shape in constructing the wet modes of vibration.

Table 1: Normalized modal added mass matrix for the first four mode shapes of the hemispherical shell

$[m_a]_{jk}/[m]_{jj}$	$k=1$	$k=2$	$k=3$	$k=4$
$j=1$	7.95	-0.04	0.00	-0.01
$j=2$	0.03	7.95	-0.02	0.00
$j=3$	0.00	-0.02	6.26	-0.01
$j=4$	-0.02	0.00	0.01	6.25

Table 2: Eigen vector of participation factors with their associated wet frequency

	$\{\boldsymbol{Q}\}_1$	$\{\boldsymbol{Q}\}_2$	$\{\boldsymbol{Q}\}_3$	$\{\boldsymbol{Q}\}_4$
$\begin{Bmatrix} \text{dry mode 1} \\ \text{dry mode 2} \\ \text{dry mode 3} \\ \text{dry mode 4} \end{Bmatrix}$	$\begin{Bmatrix} -0.73 \\ 0.68 \\ 0.00 \\ 0.00 \end{Bmatrix}$	$\begin{Bmatrix} -0.69 \\ -0.72 \\ 0.00 \\ 0.00 \end{Bmatrix}$	$\begin{Bmatrix} 0.00 \\ 0.00 \\ 0.61 \\ 0.79 \end{Bmatrix}$	$\begin{Bmatrix} 0.00 \\ 0.00 \\ 0.78 \\ -0.62 \end{Bmatrix}$

The vectors of participation factor in Table 2 are linearly independent. The first two dry mode shapes which are associated to the first repeated frequency have dominant contributions in the first two wet mode shapes. This relationship can be observed in Fig. 3a, 3c and 3b, 3d, respectively. Similarly, wet modes 3 and 4 are constructed mainly from the third and fourth dry modes.

Table 3: Ratio between the wet and dry frequencies of the hemispherical shell

	$f_j^{*(wet)}/f_j^{*(dry)}$	$\epsilon_j = 100 \times \left(f_j^{*(dry)} - f_j^{*(wet)}\right)/f_j^{*(dry)}$
$j=1$	0.33	66.65%
$j=2$	0.33	66.50%
$j=3$	0.37	62.83%
$j=4$	0.37	62.92%

The ratio of dry and wet frequencies and the relative downshift ϵ_j in natural frequency due to fluid added-mass effect are reported in Table 3. For all the modes, the wet frequencies are lower than their dry counterparts, demonstrating the additional resistance from fluid motion induced by the deflection of the interface. The considerable reduction in the frequencies implies the significant impact of fluid loading on the vibration response of such shell structures.

Table 4: Normalized modal added damping matrix for the first four mode shapes of the hemispherical shell

$[C_a]_{jk}/\left([m]_{jj} \times f_j^{(wet)}\right)$	$k=1$	$k=2$	$k=3$	$k=4$

$j = 1$	171.93	1.90	-0.03	0.01
$j = 2$	-2.19	171.12	-0.12	-0.02
$j = 3$	-0.02	0.10	4.01	0.08
$j = 4$	0.11	0.03	-0.07	4.04

To study the forced vibration of the shell for the given external loads shown in Fig. 1b, the modal added damping, which represents the dissipative effects of the free-surface wave, were included. Table 4 shows the modal added damping which are normalized by the critical damping $[C_{cr}]_{jj} = [m]_{jj} \times f_j^{(wet)}$ with $f_j^{(wet)}$ being the wet frequency of the jth mode. It can be seen that for all the four modes, the diagonal elements of the matrix which represent the added-damping factors are all greater than one. This implies that the shell is overdamped due to the dissipative effect of the free-surface waves. The off-diagonal elements are smaller than the diagonal damping factors by at least two orders of magnitude. It is noted that the modal damping tends to be larger at lower frequencies, and the added damping is the same for mode shapes associated with repeated frequencies.

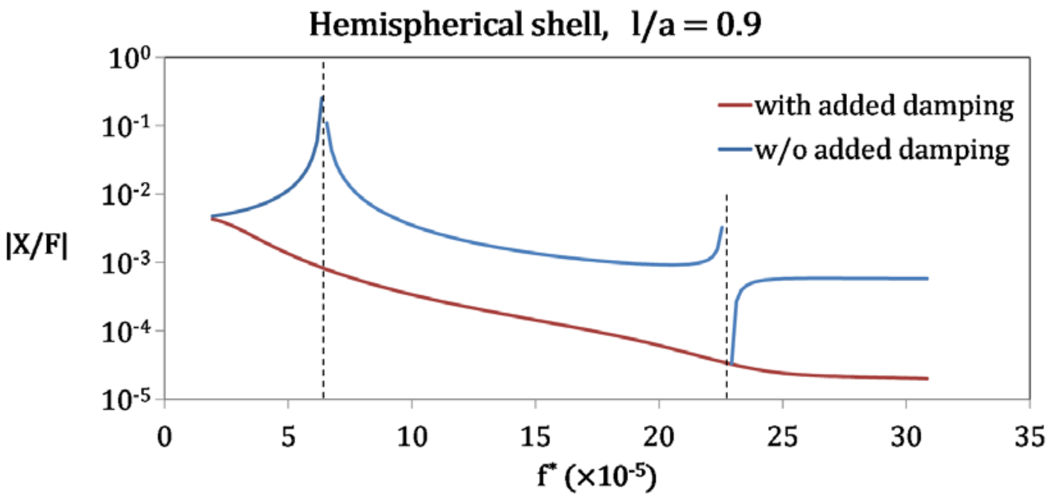

Figure 4: Forced vibration response of the hemispherical shell subjected to force F at point P, as shown in Fig. 1b, with and without including the added damping form the free-surface wave effect.

The displacement response at an observation point P due to the given load over a frequency range that contains the two natural frequencies is plotted in Fig. 4. The results are shown for two cases, with and without free-surface wave effect, to investigate the added-damping. When the surface wave was neglected, strong resonance can be observed when the excitation frequency approaches the calculated natural wet frequencies. By including the free-surface wave and hence its added-damping effect, the vibration response shows that the system is in the overdamped state as the free-surface wave carried energy away from the shell. This implies that resonance will not occur in this frequency range as long as the shell is partially submerged in a fluid.

For the next case study, a simplified ship model was developed for analysis, as shown in Fig. 5. The model dimensions are 200m (length)$\times$30m (width) $\times$15m (height). Three plate partitions with 10 m height were placed inside hull at 40, 100 and 160 m. The ship draft is considered to be 10 m, which is illustrated by a horizontal line on the ship hull. Two equal and opposite forces shown in Fig. 5b are exerted on the sides of ship hull for forced vibration analysis.

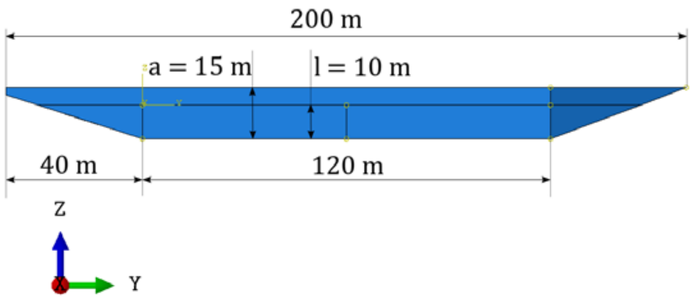

(a)

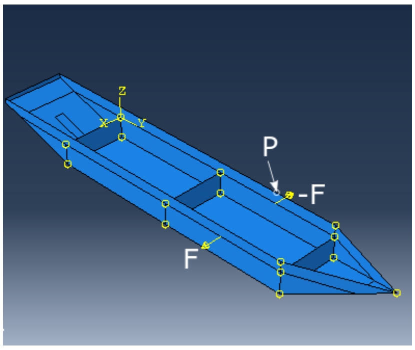

(b)

Figure 5: (a) schematic illustration of a simplified ship model, immersed partially by l and (b) the location of external forces acting on the side walls for forced vibration study

The first four dry frequencies and mode-shapes of the ship model were obtained using finite element analysis. Similar to the previous case, the fluid loading was calculated for each dry mode-shape by using the Boundary Element Method, with and without including the free-surface wave effects. After deriving the added mass matrix, the free vibration of the wet ship model was solved to obtain the wet mode-shapes and natural frequencies. It is noted the internal plates in the model were not considered in fluid flow simulation, since only the fluid-solid interface is required. However, the stiffeners affect the dry mode shapes and consequently the fluid pressure experienced by the ship structure.

Fig. 6 shows the first four dry and wet mode-shapes of the ship model. The first four wet modes were closely related to the corresponding first four dry modes, indicated by the dominant contributing factor. Direct correspondence between the dry and wet mode-shapes shows that the choice of modes for modal superposition is appropriate and no further iteration is required in this numerical algorithm. The normalized frequencies are also reported for each mode. As expected, the wet frequencies are lower than the dry ones by one order of magnitude. This implies that the impact of the fluid added-mass is considerable for this type of structure.

Fig. 7 shows the response of the ship at an observation point P due to the given excitation force over a range of frequencies. In the first scenario, the free-surface wave is neglected to detect the resonance occurrence by performing a frequency sweep, as shown by the blue solid line and markers. The second scenario with the damping from the free-surface wave was then conducted with the forced vibration analysis. The displacement results show slightly lower displacement amplitudes compared to the undamped case, indicating that the structure is underdamped. It can be inferred that the free-surface wave only dissipates a small fraction of the vibration energy from the ship within this range of excitation frequencies. This is in contrast with the overdamped case of the hemisphere discussed previously. Thus, it is concluded that including the free-surface wave may result in either underdamped, critically damped, or overdamped vibration, depending on the displacement profile of the mode-shapes. From Table 5, it can be verified that the forced vibration response of the ship is indeed underdamped since all the added damping factors are smaller than one.

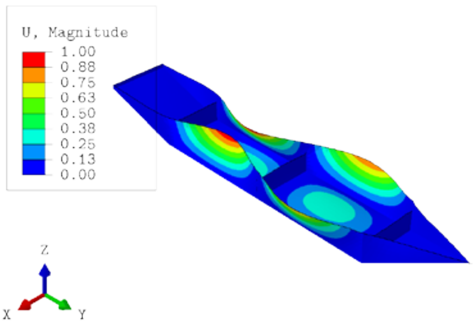

(a) 1st dry mode shape, $f_j^* = 8.56 \times 10^{-5}$

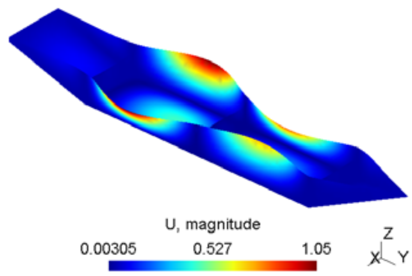

(b) 1st wet mode shape, $f_j^* = 7.28 \times 10^{-6}$

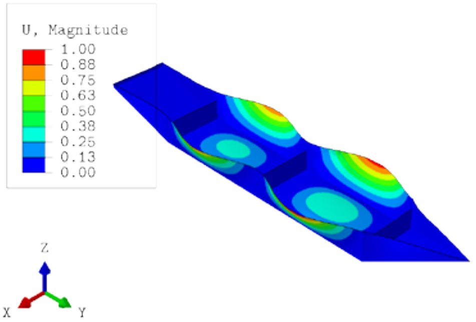

(c) 2nd dry mode shape, $f_j^* = 9.37 \times 10^{-5}$

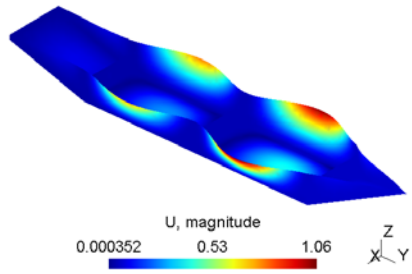

(d) 2nd wet mode shape, $f_j^* = 8.39 \times 10^{-6}$

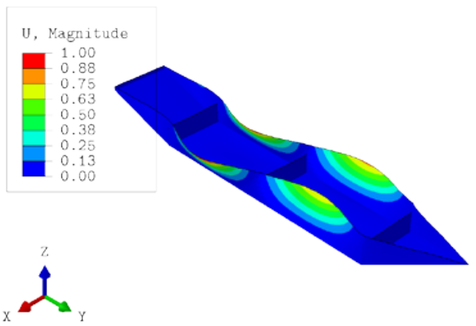

(e) 3rd dry mode shape, $f_j^* = 11.1 \times 10^{-5}$

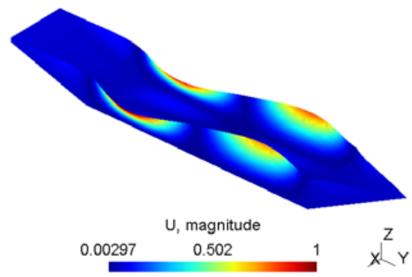

(f) 3rd dry mode shape, $f_j^* = 13.54 \times 10^{-6}$

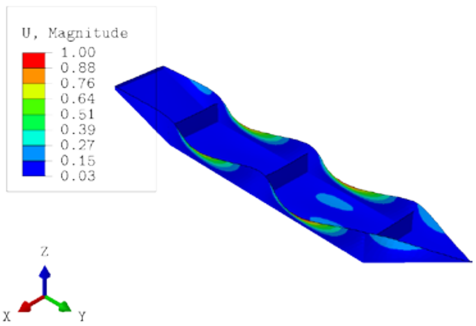

(g) 4th dry mode shape, $f_j^* = 12.5 \times 10^{-5}$

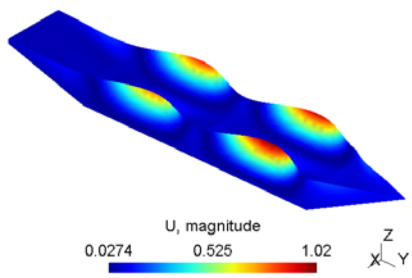

(h) 4th wet mode shape, $f_j^* = 16.90 \times 10^{-6}$

Figure 6: Panels (a), (c), (e) and (g) are the first four dry mode shapes of a simplified ship model with internal plate partitions and panels (b), (d), (f) and (h) are their wet counterparts, respectively, for the immersion depth of $\hat{l} = 2/3$

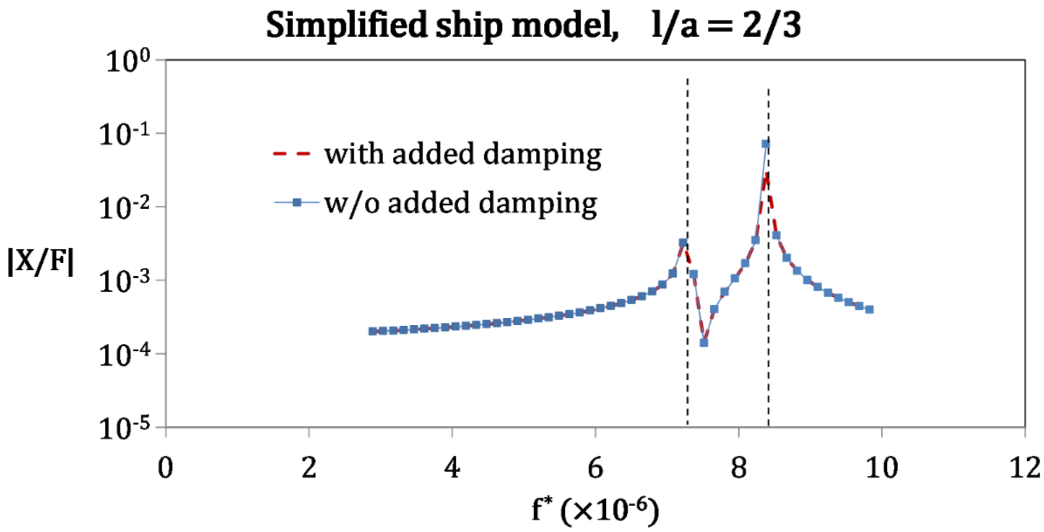

Figure 7: Forced vibration response of the simplified ship model subjected to force F at point P, as shown in Fig. 5b, with and without including the added damping form the free-surface wave effect.

Table 5: Normalized modal added damping matrix for the first four mode shapes of the simplified ship model

$[C_a]_{jk}/\left([m]_{jj} \times f_j^{(wet)}\right)$	$k = 1$	$k = 2$	$k = 3$	$k = 4$
$j = 1$	5.3×10^-3	-0.03	0.00	0.01
$j = 2$	-0.02	0.20	0.02	-0.06
$j = 3$	0.00	0.01	1.5×10^-3	0.00
$j = 4$	0.00	-0.05	0.00	0.02

Discussion

The added damping due to the free-surface wave represents a part of vibrational energy that is carried away from the structure. The added-damping may be neglected for free vibration analysis since the purpose is to determine only the natural frequencies. The natural frequencies are functions of mass and stiffness only. However, for steady-state forced vibration analysis, it is necessary to include the added-damping effect.

Conclusions

The proposed numerical algorithm for structural vibration interacting with a fluid combines the use of finite element method, boundary element method and modal superposition. Finite element solver is used to derive the mode-shapes of structure in the absence of fluid (dry modes). Modal superposition is applied to reduce the problem size and calculate the partial fluid loading. The boundary element method is used to calculate the fluid loading, for two scenarios of with and without free-surface waves. A numerical implementation of the modified Green's function was proposed to impose the free-surface wave condition automatically. This ensures that only the fluid-structure interface needs to be discretized for the Boundary Element simulation, leading to a much smaller problem-size.

The proposed numerical scheme was used to study the vibration response of a partially submerged hemispherical shell and simplified ship structure. The results showed the impact of modal added mass on lowering the natural frequencies of vibration. It was also shown that added-damping is large for the hemisphere at low frequencies. The simplified model of a ship structure was used to study the effects of fluid added-mass and damping for more practical applications. It was demonstrated that the fluid added-mass is significantly larger than the structural modal mass, especially for the lower modes. The proposed formulation provides an efficient algorithm for solving forced vibration problems of fluid-structure interaction since the problem size is reduced to the number of selected mode shapes.

Acknowledgement: This study is supported by the Singapore Maritime Institute (Project ID: SMI-2015-MA-08).

References

[1] Newman, J. N. (1979), The theory of ship motions, *Advances in applied mechanics* **18**, 221–283.
[2] Brennen C. E. (1982) A Review of Added Mass and Fluid Inertial Forces. Naval Civil Engineering Laboratory, Sierra Madre CA
[3] Korotkin A. I. (2008) Added masses of ship structures. Springer Science & Business Media **88**.
[4] Yeung, R. W. (1981) Added mass and damping of a vertical cylinder in finite-depth waters, *Applied Ocean Research* **3** (3) 119–133.
[5] Evans, D. V., McIver, P. (1984) Added mass and damping of a sphere section in heave, *Applied Ocean Research* **6** (1) 45–53.
[6] Rahman, M., Bhatta, D. D. (1993) Evaluation of added mass and damping coefficient of an oscillating circular cylinder, *Applied Mathematical Modelling* **17** (2) 70–79.
[7] Conca, C., Osses, A., Planchard, J. (1997) Added mass and damping in fluid-structure interaction, *Computer methods in applied mechanics and engineering* **146** (3-4) 387–405.
[8] Lopes, D. B. S., Sarmento, A. (2002) Hydrodynamic coefficients of a submerged pulsating sphere in finite depth, *Ocean engineering* **29** (11) 1391–1398.
[9] Sutulo, S., Rodrigues, J. M., Soares, C. G. (2009) Computation of inertial and damping characteristics of ship sections in shallow water, *Ocean Engineering* **36** (14) 1098–1111.
[10] Sutulo, S., Rodrigues, J. M., Soares, C. G. (2010) Hydrodynamic characteristics of ship sections in shallow water with complex bottom geometry, *Ocean Engineering* **37** (10) 947–958.
[11] Newman, J. N. (1984) Approximations for the Bessel and Struve functions, *Mathematics of Computation* **43** (168) 551–556.
[12] Liapis, S. (1992) Numerical methods for water-wave radiation problems, *International journal for numerical methods in fluids* **15** (1) 83–97.
[13] B. Ponizy, B., Noblesse, F., Ba, M., Guilbaud, M. (1994) Numerical evaluation of free-surface green functions, *Journal of Ship Research* **38** (3) 193–202.
[14] Chen, G.-R., Fang, M.-C. (2001) Hydrodynamic interactions between two ships advancing in waves, *Ocean Engineering* **28** (8) 1053–1078.
[15] Kim, B., Shin, Y. S. (2003) A NURBS panel method for three-dimensional radiation and diffraction problems, *Journal of ship research* **47** (2) 177–186.
[16] Noblesse, F., Huang, F., Yang, C. (2013) The Neumann–Michell theory of ship waves, *Journal of Engineering Mathematics* **79** (1) 51–71.
[17] Peter, M. A., Meylan, M. H. (2004) The Eigenfunction expansion of the infinite depth free surface Green function in three dimensions, *Wave Motion* **40** (1) 1–11.
[18] Wang, C. D., Meylan, M. H. (2004) A higher-order-coupled boundary element and finite element method for the wave forcing of a floating elastic plate, *Journal of Fluids and Structures* **19** (4) 557–572.
[19] Ergin, A., Temarel, P. (2002) Free vibration of a partially liquid-filled and submerged, horizontal cylindrical shell, *Journal of Sound and vibration* **254** (5) 951–965.
[20] Ergin, A., Price, W. G. (1992) Dynamic characteristics of a submerged, flexible cylinder vibrating in finite water depths, *Journal of Ship Research* **36** (1992) 154–167.
[21] Chen, S. S., Wambsganss, M. W., Jendrzejczyk, J. A. (1976) Added mass and damping of a vibrating rod in confined viscous fluids, *Journal of Applied Mechanics* **43** (2) 325–329.
[22] Haddara, M. R., Cao, S. (1996) A study of the dynamic response of submerged rectangular flat plates, *Marine Structures* **9** (10) 913–933.
[23] Chang, T.-P., Liu, M.-F., (2000) On the natural frequency of a rectangular isotropic plate in contact with fluid, *Journal of Sound and Vibration* **236** 547–553.
[24] Sepehrirahnama, S., Wijaya, F. B., Ong, E. T., Lee, H. P., Lim, K.-M. (2018) Modal added mass for flexural vibration of floating structures, Applied Ocean Research (submitted)
[25] Craik, A. D. D. (2004) The origins of water wave theory, *Annual Review of Fluid Mechanics* **36** 1–28.
[26] Abramowitz M, Stegun I. A. (1965) Handbook of mathematical functions with formulas, graphs, and mathematical table, New York: Dover